JCI insight

Differential effects of PD-L1 versus PD-1 blockade on myeloid inflammation in human cancer

Noffar Bar, … , Kavita M. Dhodapkar, Madhav Dhodapkar

JCI Insight. 2020. https://doi.org/10.1172/jci.insight.129353.

Clinical Medicine In-Press Preview Hematology Immunology

Introduction:

PD-1 and PD-L1 have been studied interchangeably in the clinic as checkpoints to reinvigorate T cells in diverse tumor types. Data for biologic effects of checkpoint blockade in human premalignancy are limited.

Methods:

We analyzed the immunologic effects of PD-L1 blockade in a clinical trial of atezolizumab in patients with asymptomatic multiple myeloma (AMM), a precursor to clinical malignancy. Genomic signatures of PD-L1 blockade in purified monocytes and T cells in vivo were also compared to those following PD-1 blockade in lung cancer patients. Effects of PD-L1 blockade on monocyte-derived dendritic cells were analyzed to better understand its effects on myeloid antigen-presenting cells.

Results:

In contrast to anti-PD-1 therapy, anti-PD-L1 therapy led to a distinct inflammatory signature in CD14+ monocytes and increase in myeloid-derived cytokines (e.g. IL-18) in vivo. Treatment of AMM patients with atezolizumab led to rapid activation and expansion of circulating myeloid cells which persisted in the bone marrow. Blockade of PD-L1 on purified monocyte-derived dendritic cells (DCs) led to rapid inflammasome activation and synergized with CD40L-driven DC maturation, leading to greater antigen-specific T cell expansion.

Conclusions:

These data show that PD-L1 blockade leads to distinct systemic […]

Differential effects of PD-L1 versus PD-1 blockade on myeloid inflammation in human cancer

Noffar Bar[1]*, Federica Costa[2,3]*, Rituparna Das[2]*, Alyssa Duffy[2]*, Mehmet Samur[4], Samuel McCachren[2], Scott N. Gettinger[1], Natalia Neparidze[1], Terri L. Parker[1], Jithendra Kini Bailur[2], Katherine Pendleton[2,5], Richa Bajpai[2], Lin Zhang[1], Mina L. Xu[6], Tara Anderson[1], Nicola Giuliani[3], Ajay Nooka[2], Hearn J. Cho[7], Aparna Raval[8], Mala Shanmugam[2,9], Kavita M. Dhodapkar[#5,9], Madhav V. Dhodapkar[#2,9]

Department of [1]Medicine and [6]Pathology, Yale University School of Medicine, New Haven, CT
[2]Department of Hematology/Oncology, Emory University, Atlanta, GA
[3]Department of Medicine and Surgery, University of Parma, Parma, Italy
[4]Department of Data Sciences, Dana-Farber Cancer Institute, Boston, MA
[5]Department of Pediatrics, Children's Healthcare of Atlanta, Emory University, Atlanta, GA
[7]Mount Sinai Medical Center, New York, NY
[8]Oncology Biomarker Development, Genentech, South San Francisco, CA
[9]Winship Cancer Institute, Emory University, Atlanta, GA

*Share first authorship (alphabetical order)
#Share senior authorship

Running title: PD-L1 versus PD-1 blockade on myeloid inflammation
Key Words: PD-L1, myeloid, smoldering myeloma, prevention, lung cancer

Conflict of interest: AR is an employee of Genentech. Remaining authors report no conflict of interest.

Correspondence:
Madhav V. Dhodapkar, MD
E-mail: madhav.v.dhodapkar@emory.edu
OR
Kavita M. Dhodapkar, MD
E-mail: kavita.dhodapkar@emory.edu

Abstract:

Introduction:

PD-1 and PD-L1 have been studied interchangeably in the clinic as checkpoints to reinvigorate T cells in diverse tumor types. Data for biologic effects of checkpoint blockade in human premalignancy are limited.

Methods:

We analyzed the immunologic effects of PD-L1 blockade in a clinical trial of atezolizumab in patients with asymptomatic multiple myeloma (AMM), a precursor to clinical malignancy. Genomic signatures of PD-L1 blockade in purified monocytes and T cells in vivo were also compared to those following PD-1 blockade in lung cancer patients. Effects of PD-L1 blockade on monocyte-derived dendritic cells were analyzed to better understand its effects on myeloid antigen-presenting cells.

Results:

In contrast to anti-PD-1 therapy, anti-PD-L1 therapy led to a distinct inflammatory signature in CD14+ monocytes and increase in myeloid-derived cytokines (e.g. IL-18) in vivo. Treatment of AMM patients with atezolizumab led to rapid activation and expansion of circulating myeloid cells which persisted in the bone marrow. Blockade of PD-L1 on purified monocyte-derived dendritic cells (DCs) led to rapid inflammasome activation and synergized with CD40L-driven DC maturation, leading to greater antigen-specific T cell expansion.

Conclusions:

These data show that PD-L1 blockade leads to distinct systemic immunologic effects compared to PD-1 blockade in vivo in humans, particularly manifest as rapid myeloid activation. These findings also suggest an additional role for PD-L1 as a checkpoint for regulating inflammatory phenotype of myeloid cells and antigen-presentation in DCs, which may be harnessed to improve PD-L1-based combination therapies.

Trial Registration: NCT02784483

Funding: NCI CA197603, CA238471, CA208328

Introduction:

Antibody-mediated blockade of PD-1 or PD-L1 has led to tumor regression and improved survival in a subset of patients with diverse tumor types (1). PD-L1-expressing tumor cells and antigen-presenting cells (APCs) engage PD-1+ T cells, leading to T cell dysfunction. In view of the dominant role of T cells in tumor immunity, blockade of PD-1 or PD-L1 has been studied interchangeably in clinical cancer immunotherapy as a strategy to activate T cells. However both molecules have alternate ligands/receptors; it has also been suggested that PD-L1 can act as a receptor to back-transmit signals into T cells (2) and tumor cells (3). PD-L1 is constitutively expressed on a subset of myeloid antigen-presenting cells (APCs) including dendritic cells (DCs) and prior studies in murine models have suggested functional role for PD-L1 in myeloid cells or DCs (4-6). Direct comparison of signaling pathways altered in vivo following PD-1 or PD-L1 blockade in T cells and APCs in humans are limited and may help optimal design of combination therapies with these antibodies. While PD-L1 axis has been extensively studied in the context of immunotherapy of established cancer, data about the effects of PD-L1 blockade on premalignant states are limited.

Multiple myeloma (MM) is a common hematologic malignancy, which is preceded in all cases by well-defined precursor states, monoclonal gammopathy of undetermined significance (MGUS) and asymptomatic multiple myeloma (AMM) (7). In spite of major therapeutic advances, there is an unmet need to achieve durable unmaintained responses in this malignancy, prompting the need to pursue strategies to engage long-term immunologic memory against tumor cells. Antibody-mediated blockade of PD-1 as a single agent did not lead to tumor regression in relapsed MM (8). Prior studies have demonstrated immune recognition of preneoplastic MGUS cells by T cells (9, 10). In a prospective trial, the presence of pre-existing T cell immunity to an embryonal stem cell antigen SOX2 was associated with reduced risk of progression to clinical MM (11). MM tumor cells commonly express PD-L1 and the expression of PD-L1 on MGUS/AMM cells correlated with an increased risk of transformation to clinical malignancy (11, 12). These considerations prompted us to initiate a clinical trial of single agent anti-PD-L1 antibody (atezolizumab) in patients with AMM (Figure 1B).

Results:

Prior studies have shown that therapy with anti-CTLA-4, anti-PD-1, or combination leads to distinct genomic signatures in purified human T cells and monocytes in vivo (13). In order to compare the genomic and proteomic profiles of anti-PD-1 and anti-PD-L1 therapies, we isolated T cells and CD14+ monocytes from peripheral blood prior to and after anti-PD-L1 therapy in patients with advanced non-small cell lung cancer and analyzed changes in gene expression utilizing Affymetrix HTA v2.0 array. In direct contrast to prior studies with anti-PD-1 therapy which predominantly leads to gene expression changes in T cells (13), anti-PD-L1 therapy led to dominant gene expression changes in CD14+ monocytes (Figure 2A). Importantly, changes in gene expression following anti-PD-L1 therapy in both T cells and monocytes were non-overlapping with those observed following anti-PD-1 therapy (Figure 2A). Top differentially expressed genes (DEG) in myeloid cells following PD-L1 blockade included inflammation-associated genes such as HBEGF (heparin-binding EGF-like growth factor), thrombospondin-1 (THBS), IL1β, CXCL1/GROα, CXCL2 and NLRP3 (Figure 2B). Pathway analysis of DEGs ($q < 0.01$) in monocytes revealed pathways related to inflammation and inflammasome-associated cytokines (IL-1 and IL-18) (supplementary table S1). In order to further validate these data in the context of samples analyzed together and determine if these signals were derived from only a subset of monocytes, we analyzed purified monocytes from patients before/after anti-PD1/PD-L1 therapy utilizing single cell RNA sequencing. These data demonstrated that early changes in myeloid cells were again more prominent following PD-L1 blockade (Figure 2C) and involved nearly all classical monocytes (Figure 2D). Changes in gene expression in these monocytes were similar to those in earlier studies (supplementary Figure S1A), and also revealed pathways consistent with myeloid activation (supplementary Figure S1B). Analysis of sera before/after therapy demonstrated that while both therapies led to an increase in IP-10 as a marker of immune activation, increase in serum IL-18, GROα, IFNα2 typically derived from myeloid cells and sCD40L, is only observed following anti-PD-L1 therapy (Figure 3A-E). Taken together, these data demonstrate that systemic immunologic changes following anti-PD-L1 therapy are surprisingly distinct from that following anti-PD-1 therapy, both at genomic and proteomic levels, in particular with rapid activation of inflammation-associated genes in monocytes.

Expression of PD-L1 was previously correlated with the risk of progression to MM (11). In order to evaluate the potential of targeting PD-L1 axis to prevent MM, we enrolled AMM patients in a pilot trial of single agent atezolizumab. The trial was closed prematurely based on FDA guidance after enrollment of only 2 patients due to safety concerns emerging in two clinical trials of pembrolizumab and lenalidomide in MM. Clinical data from these patients are summarized in supplementary table S2. Both patients had stable disease at the time of study closure, after receiving 7 and 1 cycles

respectively, and remain progression-free off therapy with 23 and 18 month follow-up. Patient #1 developed grade 2 endocrinopathy with hypothyroidism and adrenal insufficiency after 7 cycles. Incidentally, this patient also experienced remission of prior gluten intolerance after enrolling on study. Serial analysis of peripheral blood samples by mass cytometry revealed an early increase in blood monocytes and decline in B cells in both patients, detected at 15 days after initiation of therapy (C1D15) (Figure 4A and supplementary Figure S2A). Phenotypic analysis revealed an increase in $CD16^{+}CD40^{+}HLADR^{hi}$ monocytes (Figure 4B). In order to validate these findings in an independent dataset, we analyzed early changes in blood monocytes from another clinical trial in MM (NCT02431208), wherein a cohort received single agent atezolizumab. These data also corroborated our prior studies and demonstrated similar pattern of rapid increase in circulating activated monocytes in vivo (Figure 4C). Taken together, data from both lung cancer and MM patients show that PD-L1 blockade leads to early activation of myeloid cells with a transient increase in activated circulating monocytes in vivo.

Evaluation of T cells in AMM patients treated with atezolizumab revealed an early increase in circulating CD8+ and CD4+ memory T cells detectable by cycle1 day15 (C1D15) (Figure 5A and supplementary Figure S2B). Single cell mass cytometry revealed proliferation of CD8+ and CD4+ effector memory (T_{EM}) compartment as well CD8+ central memory (T_{CM}) compartment manifest as upregulation of Ki-67 (Figure 5B). In prior studies, we have shown SOX2 is a common antigenic target of T cells in MGUS (10). Evaluation of antigen-specific T cells at C1D15 also revealed an increase in antigen-reactive IP10 production following stimulation with SOX2-peptide library (Figure 5C). However, therapy-induced changes in circulating T cells were transient and returned to baseline by cycle 2. Although the number of total B cells declined, therapy was also associated with an increase in $CD21^{lo}$ B cell subset implicated in autoimmunity (14) (supplementary Figure S2C). Analysis of serum cytokines also revealed early but transient changes in inflammatory cytokines (IL-18, IP-10, GROα and TNFα), which returned closer to baseline by cycle 2 (supplementary Figure S3). Together these data show that atezolizumab leads to rapid but only transient systemic immune activation in vivo in AMM patients.

Evaluation of post-treatment bone marrow specimens was planned after the completion of 2 cycles and therefore was obtained in only one patient. Post-treatment bone marrow revealed a decline in T and B cells but clear increase in the proportion of CD14+ myeloid cells (Figure 6A-B), which also exhibited some evidence of activation manifest with upregulation of HLA-DR (Figure 6C). Although reduced in number, bone marrow memory T cells from post-treatment biopsies did demonstrate an increase in granzyme and T-bet relative to baseline samples particularly within the T_{EM} subset (Figure 6D).

In order to understand the observed changes in immune cells in further detail, we analyzed single cell transcriptomes of circulating as well as bone marrow mononuclear cells. In the bone marrow, scRNA-seq identified six major T/NK cell clusters (Figure 7A-B). Of these, the proportion of T cell clusters 0 and 3 declined in the post-treatment biopsy, consistent with reduction in T cells detected by mass cytometry. In contrast, there was an increase in the proportion of cells in several myeloid clusters, including classical CD14+ myeloid cells (clusters 5), CD16+ myeloid cells (cluster 7) and dendritic cells (cluster 8). Pathways analysis of DEGs in these clusters demonstrated an increase in TNF-α signaling and IFN-α response in myeloid cells as well as other cell types, consistent with evidence of inflammatory signaling in post-treatment bone marrow (supplementary table S3). Single cell RNA sequencing analysis of paired blood samples from baseline and C1D15 from both patients also demonstrated systemic changes in gene expression, particularly in cluster 2 (myeloid cells) and cluster 5 (B cells), consistent with prior results utilizing mass cytometry (supplementary Figure S4 and supplementary table S4). Pathway analysis revealed an enrichment of interferon-response and inflammation-associated pathways post-therapy in several major circulating cell types (T cells, B cells, monocytes, and NK cells), consistent with systemic immune activation and changes in serum cytokines at this time point (supplementary table S4).

Among myeloid cells, DCs constitutively express high levels of PD-L1. Prior studies have mostly focused on effects of PD-L1 blockade in the context of DC:T cell interactions (1). In order to test if PD-L1 may directly impact the biology of human monocyte-derived DCs (Mo-DCs) independent of DC:T interactions, we cultured purified Mo-DCs with anti-PD-L1 antibodies. Culture of Mo-DCs with anti-PD-L1, but not anti-PD1 led to modest increase in CD80 and CD83 as markers of DC maturation (Figure 8A). This was associated with increase in the secretion of several inflammatory cytokines, notably IL6, IL8, TNFα and IL1β in the culture supernatants (Figure 8B), as well as rapid (within 4 hours) activation of caspase-1 (Figure 8C) and changes in cellular energetics associated with DC maturation, manifest as an increase in spare respiratory capacity (Figure 8D). In the setting of DC:T cell interaction, CD40L-mediated licensing of DCs is a critical regulator of antigen presentation(15). Therefore, we examined the impact of PD-L1 blockade on DC maturation following suboptimal concentration of CD40L. PD-L1 blockade led to increase in CD40L-driven DC maturation as detected by the expression of CD80 and CD83 (Figure 9A-B), but also greater expansion of influenza-matrix peptide (Flu-MP)-specific T cells by Flu-MP-loaded DCs (Figure 9C). Expression of PD-L1 in human Mo-DCs can vary in a donor-dependent fashion. Expression of PD-L1 on DCs correlated with the observed synergy for DC maturation with CD40L and atezolizumab (supplementary Figure S5A). In order to further evaluate the effects of PD-L1 blockade on naturally occurring bone marrow

myeloid cells, we cultured these cells with atezolizumab. Consistent with our in vivo data, atezolizumab also led to an increase in $CD16^{+}HLADR^{+}CD14^{+}$ bone marrow myeloid cells in culture (supplementary Figure S5B).

Discussion:

Together, these data demonstrate that PD-L1 blockade leads to a distinct genomic signature characterized by early activation and expansion of myeloid compartment in vivo. Therefore, while both PD1 and PD-L1 blockade share well-studied effects in terms of reinvigoration of T cells, PD-L1 blockade also unleashes an under-appreciated myeloid inflammatory checkpoint in vivo in humans. These findings are also consistent with recent data on PD-L1-mediated regulation of macrophage activation and proliferation in PD-L1-deficient mice (16).

Understanding differences between PD-1 and PD-L1 blockade will be essential for optimal design of rational combination therapies with these approaches and may differ for each of these targets. Differential effects of PD-1 versus PD-L1 blockade on myeloid cells in vivo may also help explain why PD-L1 expression on myeloid cells better predicts responsiveness to PD-L1 than PD-1 blockade in the clinic (17). PD-L1 blockade of human DCs led to rapid activation of caspase-1 / inflammasome, with upregulation of NLRP3 and inflammasome-dependent cytokines such as IL-18. Inflammasome activation plays a complex and context-dependent pro/anti-tumor role in tumor immunity (18). Activation of NLRP3-inflammasome in DCs was shown to be critical for induction of adaptive immunity to dying tumor cells following chemotherapy (19). Therefore, PD-L1 may play an important role in the afferent arm of tumor-immunity cycle in regulating antigen presentation. The finding that PD-L1 blockade may enhance CD40L/T cell-mediated DC maturation may provide the rationale for combinations of PD-L1 blockade with agents targeting agonistic CD40 signaling.

Effect of PD-L1 blockade on myeloid cells in vivo could however also have potential undesired effects. Enrichment and activation of myeloid cells following PD-L1 blockade may lead to T cell exclusion and resistance to PD-L1 blockade in myeloid-rich tumors (20). Effects on myeloid cells could also have contributed to the lack of persistent T cell activation following atezolizumab we observed in AMM patients and suggests that combinations with therapies that inhibit enrichment of myeloid compartment may be explored to improve PD-L1 blockade. Recent studies have also suggested the potential for myeloid cells to mediate hyper-progression in some tumors (21); prior studies have indeed shown the capacity of myeloid cells to promote MM growth (22, 23).

While the small number of patients treated due to regulatory issues limits interpretation, the correlative immunologic data in this earlier stage, do demonstrate the feasibility to achieve immune activation in the tumor bed. The bar for acceptable complications is lower in this setting than in clinical myeloma. Therefore, careful selection of patients

more likely to respond to immune therapies would be important for future investigations in immune-prevention based on checkpoint blockade. In this regard, recent studies show that loss of stem-like and marrow resident T cells is an early feature of MM, which may restrict the efficacy of checkpoint blockade in this setting (24). It is however notable that the finding of increase in inflammasome-dependent cytokines such as IL-18 has been prominently demonstrated in large cohorts of patients treated with anti-PD-L1 but not anti-PD-1 antibodies, which is consistent with our data (17).

An important limitation of these data is the small numbers of patients studied, due to early closure of the trial linked to regulatory concerns about PD1 pathway in a different myeloma trial. In addition, comparison between effects of PD1 and PD-L1 blockade is based on patients treated in different clinical studies, and not as a part of a prospective randomized clinical trial directly comparing PD1 and PD-L1 blockade. Such a clinical trial may now be feasible in malignancies wherein both PD1 and PD-L1 blockade are now clinically approved and would be useful to dissect biologic differences between these therapies in humans.

The finding that PD-L1 blockade leads to rapid activation of inflammatory signatures on human myeloid cells in vivo suggests that PD-L1 axis may be an important regulator of myeloid inflammation, and impact emergency myelopoiesis and trained immunity in the clinic. While studies in human subjects described here are mostly correlative, possible role of PD-L1 axis in regulating myeloid inflammation is also supported by emerging data from murine models, which is consistent with our studies. Engaging these pathways may be important for improving combination therapies with PD-L1 blockade, particularly harnessing the afferent arm of the cancer immunity cycle. Finally, differences in pharmacodynamic effects of PD1 and PD-L1 blockade as shown here, also have important implications for optimal combinations in the clinic, which may differ between these targets.

Methods:

Patients and samples:

All specimens were collected following informed consent under institutional IRB guidelines For studies comparing genomic signatures of PD-1 and PD-L1 blockade, blood samples were obtained before and after 1 cycle of therapy from patients with advanced non-small cell lung cancer undergoing therapy with anti-PD-1(nivolumab)(13) or anti-PD-L1 (atezolizumab).

Study design and monitoring:

In the pilot study of atezolizumab in AMM (NCT02788843), patients were eligible if they met criteria for AMM based on bone marrow clonal plasmacytosis of >10% and/or levels of monoclonal immunoglobulin > 3 g/dl. Patients were also required to have abnormal serum free light chain ratio (but <100) and absence of end organ damage based on CRAB criteria, <60% bone marrow plasma cells and no more than one known focal lesion on MRI. Other key eligibility criteria included the presence of measurable disease and adequate hematologic and organ function. Patients with any prior therapy for plasma cell disorder and history of active autoimmune disease were excluded. All eligible patients received atezolizumab 1200mg intravenously every 3 weeks. Blood samples for immune monitoring were collected at baseline, Cycle1day15, and then prior to each cycle of therapy while on study. Bone marrow biopsies were planned at baseline and after completion of 2 cycles of therapy.

Gene expression profiling of purified T cells and monocytes

Gene expression profiling of purified monocytes and T cells was performed as previously described(13). Briefly, CD14+ monocytes cells were isolated from peripheral blood mononuclear cells (PBMCs) using immunomagnetic separation with anti-human CD14 microbeads (Miltenyi biotec, Germany), and T cells were isolated with human Pan-T cell isolation kit (Miltenyi biotec, Germany) following manufacturer instructions. RNA isolated from purified cells was analyzed utilizing Affymetrix GeneChip Human Transcriptome Array (v2.0) as described(13).

Mass cytometry

Peripheral blood and bone marrow mononuclear cells were immunophenotypically characterized utilizing mass cytometry as described(25). The panel of antibodies utilized is shown in supplementary Table 5. Data were acquired on Helios^{TM} instrument (Fluidigm Sciences Inc.) and analyzed using Cytobank software (Cytobank Inc., Fluidigm).

Single cell RNA sequencing

Single cell RNA sequencing (sc-RNAseq) of peripheral blood or bone marrow mononuclear cells was performed using the 10X Genomics platform chromium single cell3'- kit following manufacturer's protocol as described(14, 26). Libraries were sequenced. Reads were aligned, filtered, de-duplicated, and converted into a digital count matrix using Cell Ranger 1.2 (10X Genomics). All downstream quality control and analyses were performed using Seurat(27). Cells with >=200 expressed genes were used for analysis.

For analysis of sc-RNA sequencing from lung cancer patients treated with either anti-PD-1 or PD-L1, pre- and post-treatment samples for each patient were merged, and gene expression for each cell was log-normalized to total expression per cell. To reduce noise due to batch effects and interpatient heterogeneity, each patient was aligned and integrated with all other patients receiving the same treatment (anti-PD-L1 n=3, anti-PD-1 n=4) via canonical correlation analysis (CCA) using the Seurat FindIntegrationAnchors and IntegrateData functions. Gene expression data was then scaled such that each gene had a mean expression of 0 and a variance of 1 across all cells using the ScaleData function, and principal component analysis was performed using the RunPCA function. Data was visualized in 2 dimensions using uniform manifold approximation and projection (UMAP) based on the first 20 principal components. Significantly differentially expressed genes were identified by the Wilcoxon rank-sum test with a Bonferroni correction ($p<0.05$). Cluster identity was determined by inspection of canonical marker genes (e.g., CD14 for monocytes), and identity was confirmed by automated cell type determination with SingleR via comparison to the Human Primary Cell Atlas. Pathway analysis was performed using Gene Set Enrichment Analysis (GSEA) software and the Molecular Signature Database (MSigDB) from the Broad Institute.

Whole Transcriptome Analysis

Gene expression profiles from monocytes and T cells before and after anti-PD1 and anti-PD-L1 treatment were obtained using Affymetrix Human Transcriptome Array 2.0 and gene-level signal intensities were used for subsequent analysis. Preprocessing and normalization of data sets was carried out by Affymetrix Expression Console using gene level Signal Space Transformation - Robust Multiarray Average (SST-RMA) normalization. All downstream analysis were conducted using R and Bioconductor(28). "limma" package was used for differential gene expression(29). Gene set enrichment analysis was performed using Metacore (https://portal.genego.com) and MSigDB (Molecular Signatures Database v6).

Detection of antigen-specific T cells

In order to detect SOX2-specific T cells, PBMCs were stimulated for 48 hours with SOX2 peptide library as described(10). Following stimulation, the presence of T cell

activation was determined based on the detection of IP-10 in the culture supernatant by Luminex.

Detection of plasma cytokines

Plasma samples were utilized for the detection of a panel of 38 cytokines / chemokines using Milliplex® MAP Human Cytokine/Chemokine Magnetic Bead Panel kit (HCYTMAG-60K-PX38; Millipore Sigma, USA) as described(13). xPONENT® software (Luminex Corp., USA) was used to detect, quantitate and analyze the samples on the Luminex 100™ instrument. Levels of IL18 were analyzed using an Elisa kit (R&D).

Generation of monocyte-derived dendritic cells (Mo-DCs)

Purified CD14+ monocytes were cultured in 1% plasma in the presence of IL-4 (25ng/ml; R&D Systems) and GM-CSF (20ng/ml sagramostim [Leukine]; Genzyme) to yield Mo-DCs. Immature Mo-DCs were used to study the effects of anti-PD-L1 or anti-PD-1 antibodies. DCs were cultured with anti-PD-L1 (clone 29E.2A3; Biolegend), anti-PD-1 (clone EH12.2H7; Biolegend)) or their respective isotype control antibodies (IgG2b, and IgG1; Biolegend) (200 μg/ml). For some experiments immature Mo-DCs were cultured with CD40L (250ng/ml; R&D Systems).

Effects of PD-L1 blockade on bone marrow myeloid cells

BMMNCs were treated with atezolizumab (200μg/ml) every 24 hours for 48 hours or left untreated. Following incubation, samples were stained with antibodies for CD14 (MφP9), CD19 (SJ25C1), and CD11c (B-ly6) (from BD Biosciences), BDCA3 (AD5-14H12, Miltenyi Biotec), PD-L1 (29E.2A3), CD40 (5C3), CD16 (3G8), and HLA-DR (L243) (from Biolegend).

Antigen-specific T cell stimulation.

For some experiments, immature Mo-DCs differentiated from HLA A2.1$^+$ donors (n=4) were stimulated with CD40L (250ng/ml) in the presence or absence of anti-PD-L1 (200μg/ml). After overnight culture, DCs were loaded with HLA A2.1-restricted influenza-matrix peptide (Flu-MP; sequence GILGFVFTL) at 0.1μg/ml for 2 hours. Flu-MP-loaded DCs were then used to stimulate autologous T cells at a DC/T cell ratio 1:30 in the presence of IL-2 (10 U/ml). Flow cytometry analysis was performed to detect the presence of Flu-MP-specific CD8$^+$ T cells using MHC tetramers (MBL International).

Detection of caspase-1 activation.

Immature Mo-DCs were treated with anti-PD-L1 (200μg/ml), anti-PD-1 (200μg/ml), or left untreated for 4 hours. Activation of caspase-1 was assayed with the FAM-YVAD-FMK Caspase-1 Detection Kit (Cell Technology Inc). FAM-YVAD-FMK was added to the culture 1 hour before the end of culture period, following manufacturers protocol, washed twice with Caspase-1 kit wash buffer, and detected using flow cytometry.

Measurement of oxygen consumption and spare respiratory capacity.

Basal, maximal and coupled oxygen consumption rates were measured in a Mito stress assay using a Seahorse extracellular flux (XFe96) analyzer. Immature Mo-DCs were treated with anti-PD-L1 (200μg/ml) or left untreated. After 3 hours, DCs were harvested washed 1X with PBS and plated at 200,000 cells per well in 5 -8 replicates on Cell-Tak (Becton Dickinson)-pre-coated 96 well plates custom designed for XFe96 analysis. Oxygen consumption rate was evaluated over time with sequential injection of oligomycin (final concentration 2.5μM), carbonyl cyanide p-trifluoro-methoxyphenyl hydrazone (FCCP; final concentration 0.5μM), and antimycin (Ant) or rotenone (Rot; final concentration 2μM each). Spare respiratory capacity was calculated as the difference between maximal and basal respiration.

Statistics:

Data from individual cohorts were compared using graph pad analysis software. Paired T tests and non-parametric tests were utilized to analyze the data with significance set to $p<0.05$ and Bonferroni to correct for multiple comparisons.

Study approval and monitoring

The clinical trial was approved by the Yale University institutional review board and monitored by data safety monitoring committee at Yale Cancer Center.

Author Contributions:

NB supervised the clinical trial.
FC, RD and AD designed and performed experiments.
MS and SM performed bioinformatic analysis.
SNG, NN, TLP, MLX, TA, NG, AN, HJC performed clinical research.
JKB, KP, RB, LZ, AR, MS performed some experiments.
MVD and KMD designed and performed oversight to entire project.
All authors performed data analysis and approved the final manuscript.

Acknowledgments:

This work is supported in part by funds from NIH/NCI (NCI CA197603 to MVD, CA238471 to KMD, CA208328 to MS).

References:

1. Zou W, Wolchok JD, and Chen L. PD-L1 (B7-H1) and PD-1 pathway blockade for cancer therapy: Mechanisms, response biomarkers, and combinations. *Sci Transl Med.* 2016;8(328):328rv4.
2. Dong H, Strome SE, Matteson EL, Moder KG, Flies DB, Zhu G, et al. Costimulating aberrant T cell responses by B7-H1 autoantibodies in rheumatoid arthritis. *J Clin Invest.* 2003;111(3):363-70.
3. Azuma T, Yao S, Zhu G, Flies AS, Flies SJ, and Chen L. B7-H1 is a ubiquitous antiapoptotic receptor on cancer cells. *Blood.* 2008;111(7):3635-43.
4. Curiel TJ, Wei S, Dong H, Alvarez X, Cheng P, Mottram P, et al. Blockade of B7-H1 improves myeloid dendritic cell-mediated antitumor immunity. *Nat Med.* 2003;9(5):562-7.
5. Lin H, Wei S, Hurt EM, Green MD, Zhao L, Vatan L, et al. Host expression of PD-L1 determines efficacy of PD-L1 pathway blockade-mediated tumor regression. *J Clin Invest.* 2018;128(2):805-15.
6. Tang H, Liang Y, Anders RA, Taube JM, Qiu X, Mulgaonkar A, et al. PD-L1 on host cells is essential for PD-L1 blockade-mediated tumor regression. *J Clin Invest.* 2018;128(2):580-8.
7. Dhodapkar MV. MGUS to myeloma: a mysterious gammopathy of underexplored significance. *Blood.* 2016;128(23):2599-606.
8. Lesokhin AM, Ansell SM, Armand P, Scott EC, Halwani A, Gutierrez M, et al. Nivolumab in Patients With Relapsed or Refractory Hematologic Malignancy: Preliminary Results of a Phase Ib Study. *J Clin Oncol.* 2016;34(23):2698-704.
9. Dhodapkar MV, Krasovsky J, Osman K, and Geller MD. Vigorous premalignancy-specific effector T cell response in the bone marrow of patients with monoclonal gammopathy. *J Exp Med.* 2003;198(11):1753-7.
10. Spisek R, Kukreja A, Chen LC, Matthews P, Mazumder A, Vesole D, et al. Frequent and specific immunity to the embryonal stem cell-associated antigen SOX2 in patients with monoclonal gammopathy. *J Exp Med.* 2007;204(4):831-40.
11. Dhodapkar MV, Sexton R, Das R, Dhodapkar KM, Zhang L, Sundaram R, et al. Prospective analysis of antigen-specific immunity, stem-cell antigens, and immune checkpoints in monoclonal gammopathy. *Blood.* 2015;126(22):2475-8.
12. Paiva B, Azpilikueta A, Puig N, Ocio EM, Sharma R, Oyajobi BO, et al. PD-L1/PD-1 presence in the tumor microenvironment and activity of PD-1 blockade in multiple myeloma. *Leukemia.* 2015.
13. Das R, Verma R, Sznol M, Boddupalli CS, Gettinger SN, Kluger H, et al. Combination Therapy with Anti-CTLA-4 and Anti-PD-1 Leads to Distinct Immunologic Changes In Vivo. *J Immunol.* 2015;194(3):950-9.
14. Das R, Bar N, Ferreira M, Newman AM, Zhang L, Bailur JK, et al. Early B cell changes predict autoimmunity following combination immune checkpoint blockade. *J Clin Invest.* 2018;128(2):715-20.
15. Schoenberger SP, Toes RE, van der Voort EI, Offringa R, and Melief CJ. T-cell help for cytotoxic T lymphocytes is mediated by CD40-CD40L interactions. *Nature.* 1998;393(6684):480-3.

16. Hartley GP, Chow L, Ammons DT, Wheat WH, and Dow SW. Programmed Cell Death Ligand 1 (PD-L1) Signaling Regulates Macrophage Proliferation and Activation. *Cancer Immunol Res.* 2018;6(10):1260-73.
17. Herbst RS, Soria JC, Kowanetz M, Fine GD, Hamid O, Gordon MS, et al. Predictive correlates of response to the anti-PD-L1 antibody MPDL3280A in cancer patients. *Nature.* 2014;515(7528):563-7.
18. Tartey S, and Kanneganti TD. Differential role of the NLRP3 inflammasome in infection and tumorigenesis. *Immunology.* 2019.
19. Ghiringhelli F, Apetoh L, Tesniere A, Aymeric L, Ma Y, Ortiz C, et al. Activation of the NLRP3 inflammasome in dendritic cells induces IL-1beta-dependent adaptive immunity against tumors. *Nat Med.* 2009;15(10):1170-8.
20. McDermott DF, Huseni MA, Atkins MB, Motzer RJ, Rini BI, Escudier B, et al. Clinical activity and molecular correlates of response to atezolizumab alone or in combination with bevacizumab versus sunitinib in renal cell carcinoma. *Nat Med.* 2018;24(6):749-57.
21. Lo Russo G, Moro M, Sommariva M, Cancila V, Boeri M, Centonze G, et al. Antibody-Fc/FcR Interaction on Macrophages as a Mechanism for Hyperprogressive Disease in Non-Small Cell Lung Cancer Subsequent to PD-1/PD-L1 Blockade. *Clin Cancer Res.* 2018.
22. Kukreja A, Hutchinson A, Dhodapkar K, Mazumder A, Vesole D, Angitapalli R, et al. Enhancement of clonogenicity of human multiple myeloma by dendritic cells. *J Exp Med.* 2006;203(8):1859-65.
23. Zheng Y, Cai Z, Wang S, Zhang X, Qian J, Hong S, et al. Macrophages are an abundant component of myeloma microenvironment and protect myeloma cells from chemotherapy drug-induced apoptosis. *Blood.* 2009;114(17):3625-8.
24. Bailur JK, McCachren SS, Doxie DB, Shrestha M, Pendleton KE, Nooka AK, et al. Early alterations in stem-like/resident T cells, innate and myeloid cells in the bone marrow in preneoplastic gammopathy. *JCI Insight.* 2019;5.
25. Boddupalli CS, Bar N, Kadaveru K, Krauthammer M, Pornputtapong N, Mai Z, et al. Interlesional diversity of T cell receptors in melanoma with immune checkpoints enriched in tissue-resident memory T cells. *JCI Insight.* 2016;1(21):e88955.
26. Kini Bailur J, Mehta S, Zhang L, Neparidze N, Parker T, Bar N, et al. Changes in bone marrow innate lymphoid cell subsets in monoclonal gammopathy: target for IMiD therapy. *Blood Adv.* 2017;1(25):2343-7.
27. Satija R, Farrell JA, Gennert D, Schier AF, and Regev A. Spatial reconstruction of single-cell gene expression data. *Nat Biotechnol.* 2015;33(5):495-502.
28. Huber W, Carey VJ, Gentleman R, Anders S, Carlson M, Carvalho BS, et al. Orchestrating high-throughput genomic analysis with Bioconductor. *Nat Methods.* 2015;12(2):115-21.
29. Ritchie ME, Phipson B, Wu D, Hu Y, Law CW, Shi W, et al. limma powers differential expression analyses for RNA-sequencing and microarray studies. *Nucleic Acids Res.* 2015;43(7):e47.

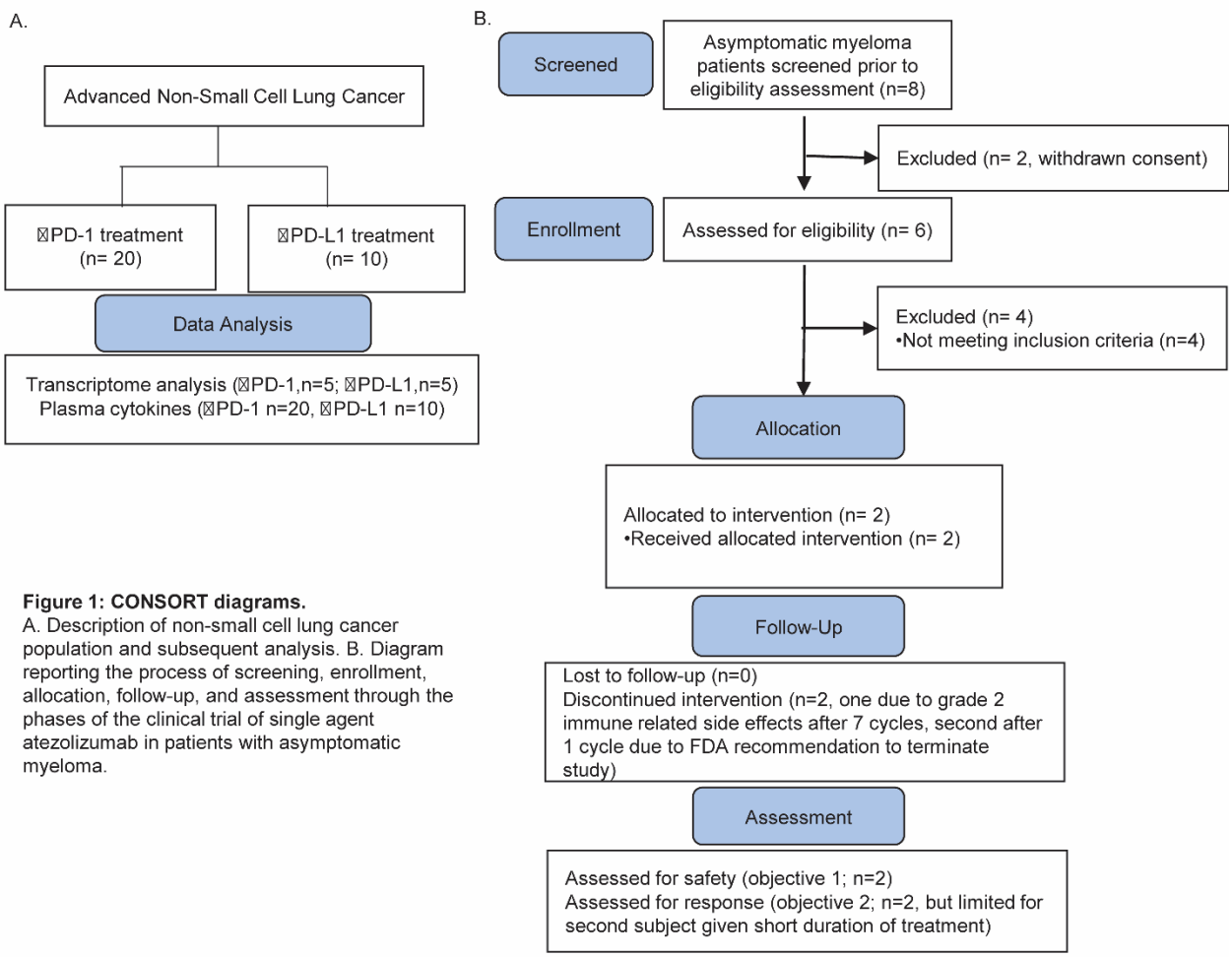

Figure 1: CONSORT diagrams.
A. Description of non-small cell lung cancer population and subsequent analysis. B. Diagram reporting the process of screening, enrollment, allocation, follow-up, and assessment through the phases of the clinical trial of single agent atezolizumab in patients with asymptomatic myeloma.

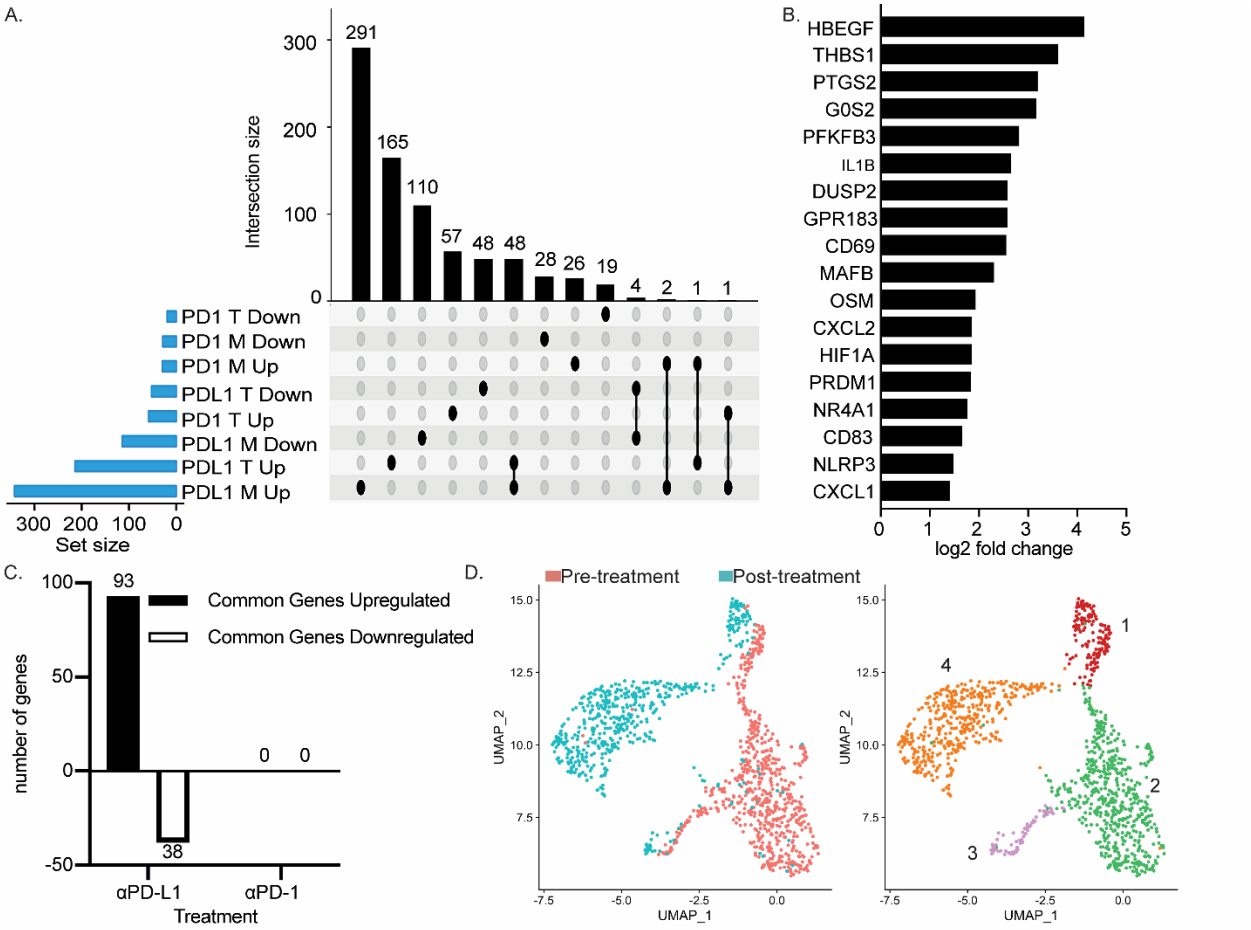

Figure 2: PD-L1 blockade leads to distinct transcriptomic changes in circulating monocytes and T cells.
RNA was extracted from magnetic bead isolated CD14+ monocytes and CD3+ T cells before and after therapy with either anti-PD-L1 (atezolizumab; n=5) or anti-PD-1 (nivolumab; n=6 previously published (10)) and analyzed using affymetrix human transcriptome array 2.0. A. Distribution of differentially regulated genes upregulated and down regulated in monocytes and T cells following therapy with anti-PD-L1 or anti-PD-1. B. Differentially regulated genes in monocytes following therapy with anti-PD-L1 (selected from top 50 differentially regulated genes). C. Single-cell RNA sequencing was performed before and after therapy with either anti-PD-L1 (n=3) or anti-PD-1 (n=4). Figure shows the number of shared differentially expressed (Wilcoxon rank-sum with Bonferroni correction $p<0.05$) genes post- vs. pre-treatment between all anti-PD-L1 treated monocytes and all anti-PD-1 treated monocytes. D. Uniform manifold approximation and projection (UMAP) plots of monocytes from single-cell RNA sequencing of anti-PD-L1 monocytes pre and post treatment (left panel, blue=post-treatment, red=pre-treatment) and monocyte groups identified by unsupervised clustering (right panel). Cluster 1=CD16+ monocytes; clusters 2, 3, and 4=CD16- monocytes.

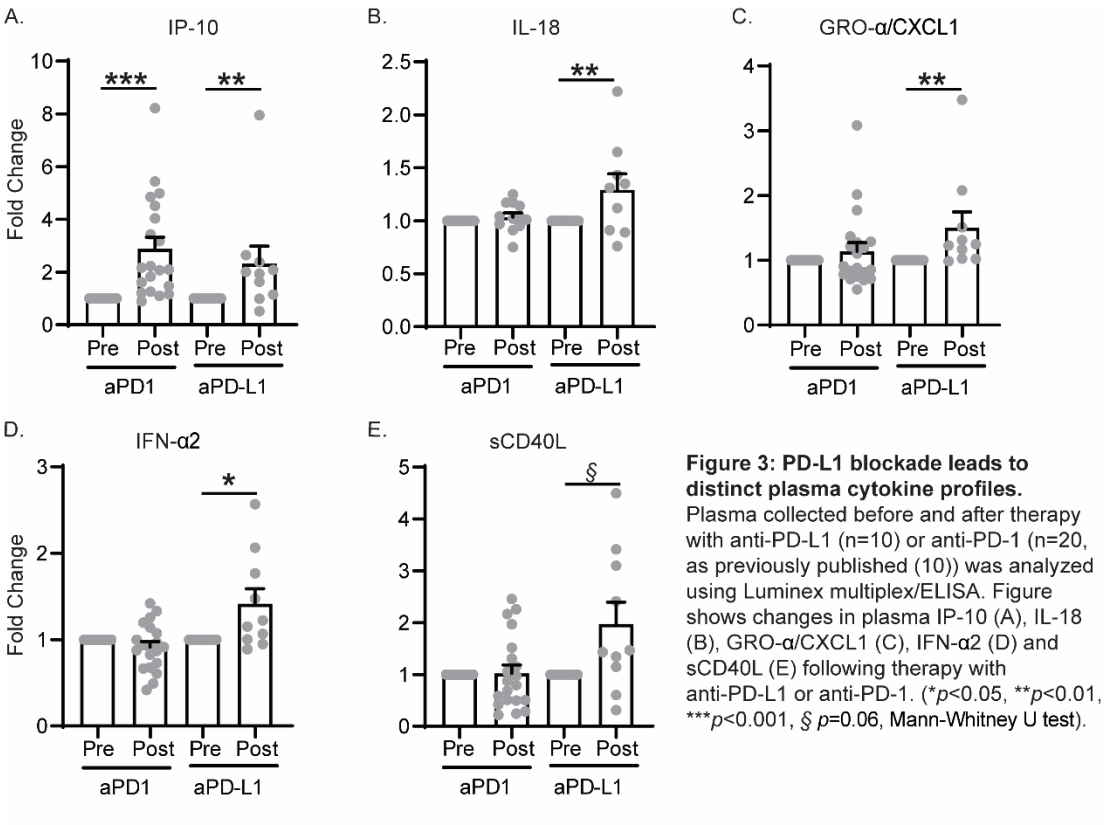

Figure 3: PD-L1 blockade leads to distinct plasma cytokine profiles. Plasma collected before and after therapy with anti-PD-L1 (n=10) or anti-PD-1 (n=20, as previously published (10)) was analyzed using Luminex multiplex/ELISA. Figure shows changes in plasma IP-10 (A), IL-18 (B), GRO-α/CXCL1 (C), IFN-α2 (D) and sCD40L (E) following therapy with anti-PD-L1 or anti-PD-1. (*p<0.05, **p<0.01, ***p<0.001, § p=0.06, Mann-Whitney U test).

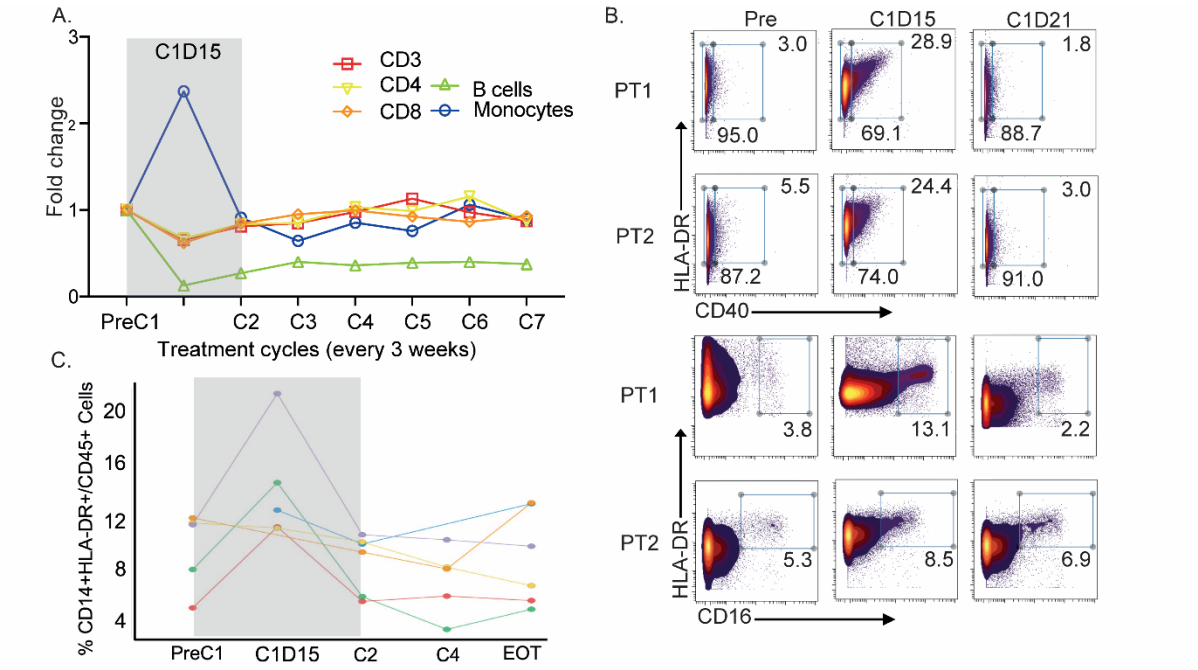

Figure 4: Changes in circulating immune cells following therapy with αPD-L1 in asymptomatic myeloma (AMM). PBMCs isolated from blood pre therapy (PreC1) and following therapy with atezolizumab on Day 15 (C1D15) as well as prior to cycles 2-7 (C2-C7) were analyzed using single cell mass cytometry or CyTOF. A. Changes in circulating CD3+, CD4+, CD8+ T cells, monocytes and B cells. Data is shown as fold change compared to pre therapy (PreC1) levels. B. Expression of CD40, HLA-DR and CD16 on circulating monocytes pre therapy (Pre) on Day 15 following first dose (C1D15) and prior to second dose of atezolizumab (C1D21) in two different patients (PT1 and PT2). C. Changes in circulating monocytes receiving atezolizumab in another clinical trial (NCT023431208). Each line represents an individual patient. EOT=end of therapy.

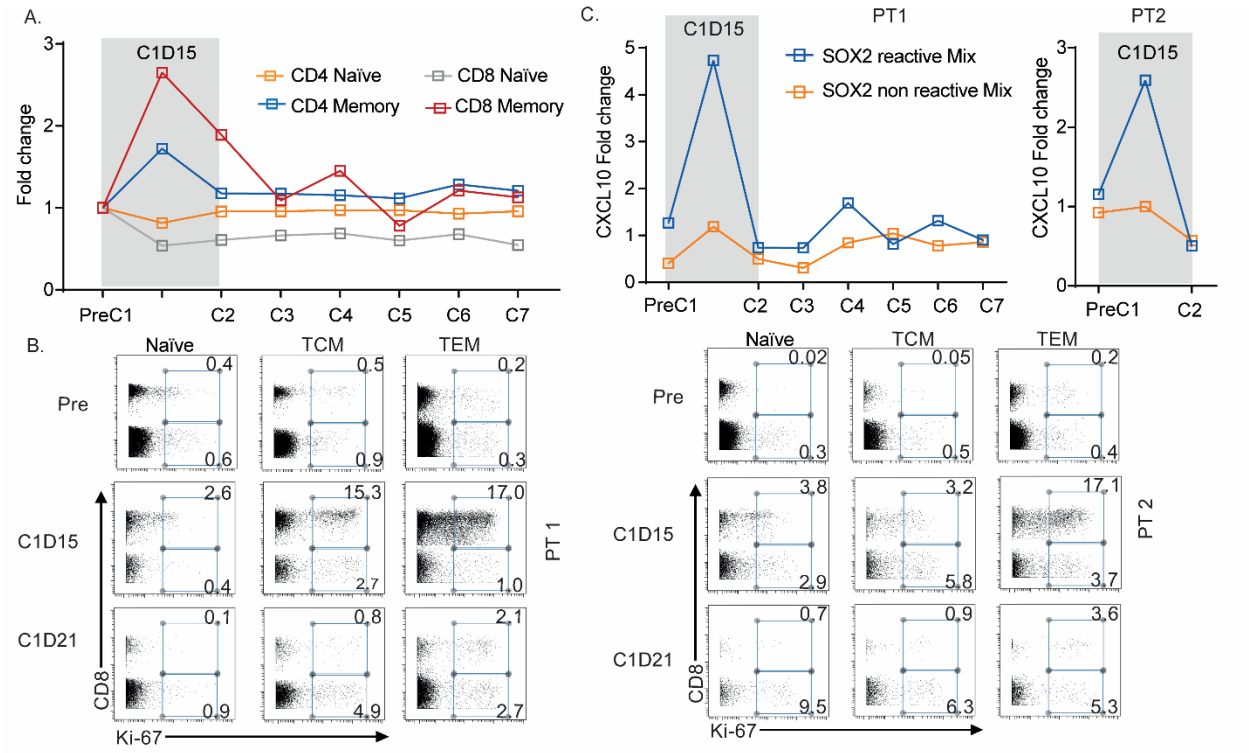

Figure 5: Changes in circulating T cells following therapy with αPD-L1 in asymptomatic myeloma (AMM).
PBMCs isolated from blood pre therapy (PreC1) and following therapy with atezolizumab on Day 15 (C1D15) as well as prior to cycles 2-7 (C2-C7) were analyzed using single cell mass cytometry or CyTOF.D.Changes in CD4 and CD8 naïve and memory T cells during therapy with atezolizumab. Data is shown as fold change compared to levels prior to starting therapy (PreC1). E. Ki-67+ proliferating naïve (CCR7+ RO-), central memory (TCM; CCR7+RO+) and effector memory (TEM; CCR7-RO+) T cells before (Pre), 15 days following start of therapy (C1D15) and prior to cycle 2 (C1D21) of therapy with atezolizumab. Figure shows data from 2 separate patients. F. PBMCs obtained pre therapy (PreC1), 15 days after starting therapy (C1D15) or prior to Cycles 2-7 (C2-C7) were evaluated for the presence of SOX2 specific T cell reactivity using overlapping peptides encompassing the entire SOX2 antigen as previously described (10). Figure shows SOX2 T cell reactivity in the two patients. Data reported as fold change compared to pre therapy (PreC1) for SOX2 reactive submix versus non reactive mix as control.

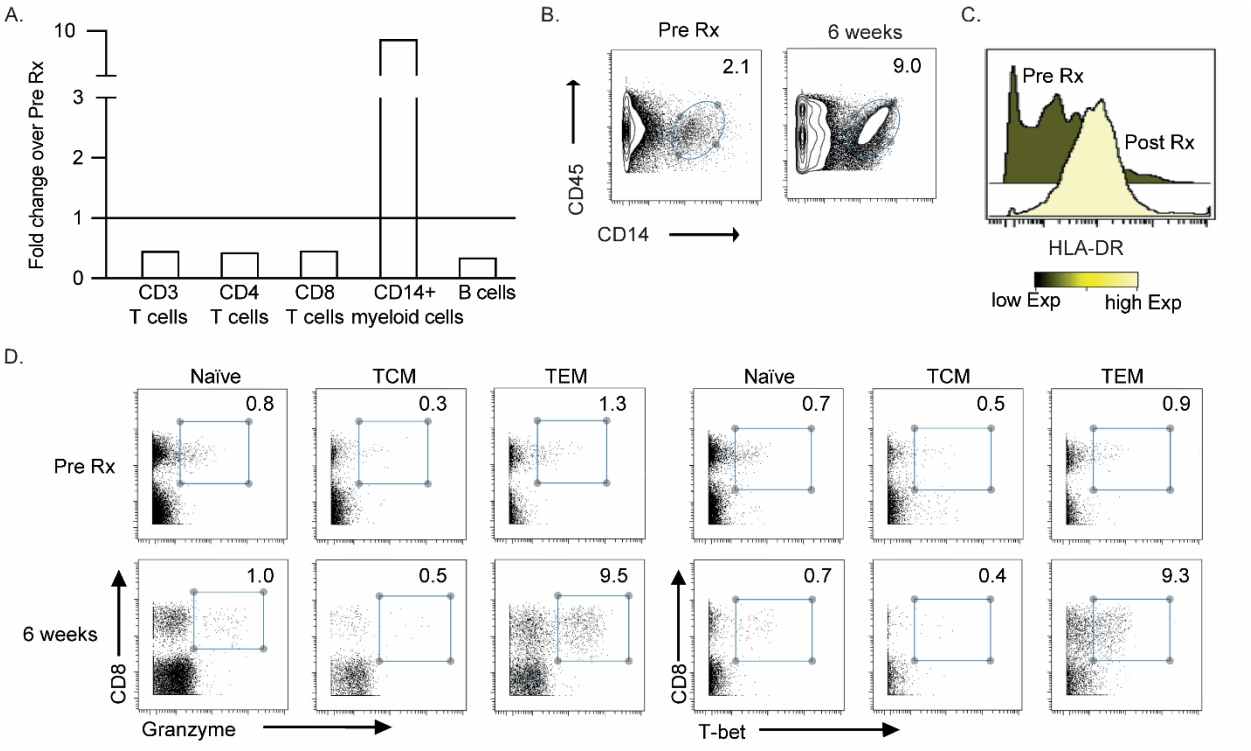

Figure 6: Changes in monocytes and effector T cells in bone marrow following therapy with αPD-L1 in AMM by mass cytometry. Bone marrow was collected from AMM patient before and after 2 cycles (6weeks) of therapy with atezolizumab. Mononuclear cells were isolated and analyzed using single cell mass cytometry. A. Bar graph shows changes in CD3, CD4, CD8 T cells, CD14+ myeloid cells and B cells at 6 weeks following therapy with atezolizumab. B. Dot plot of changes in CD14+ myeloid cells. C. Histogram showing changes in HLA-DR expression in CD14+ myeloid cells following therapy with atezolizumab. D. Proportions of Granzyme and T-bet + naïve, TCM and TEM cells in the marrow prior to start of therapy as well as 6 weeks following therapy with atezolizumab.

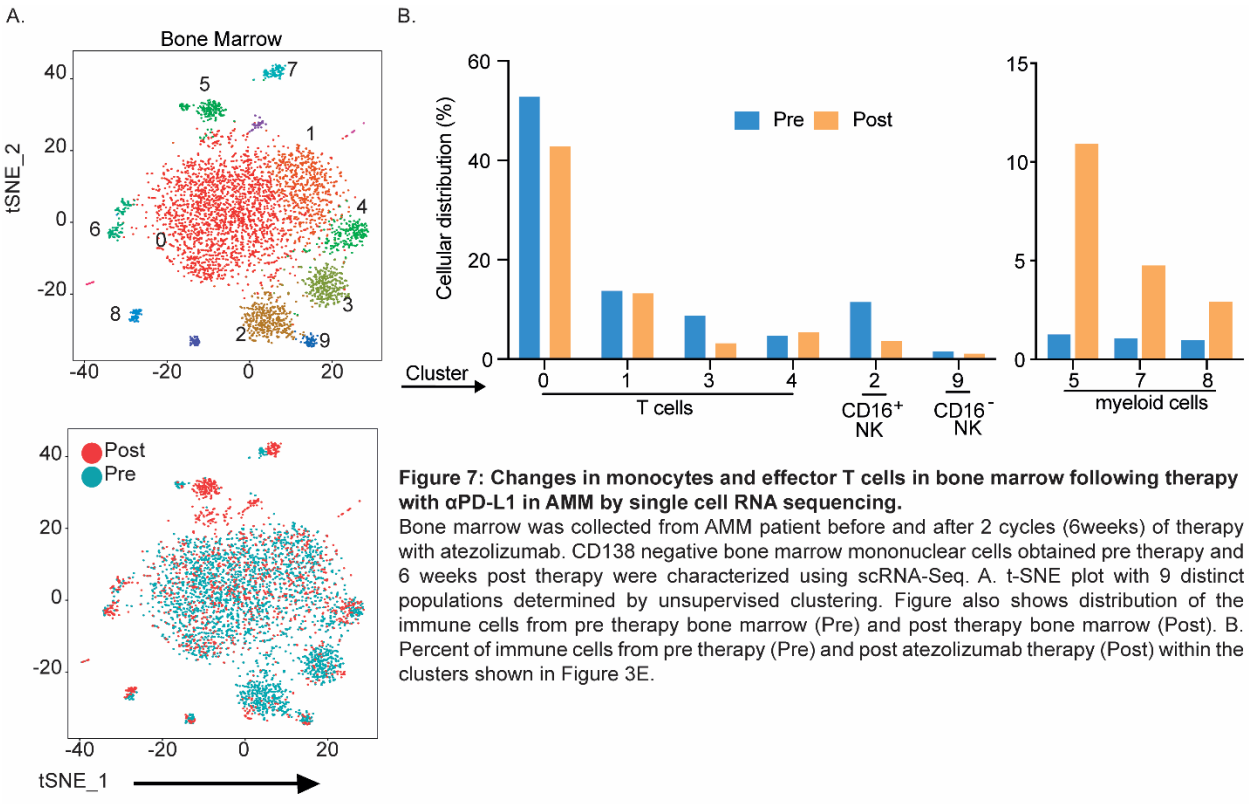

Figure 7: Changes in monocytes and effector T cells in bone marrow following therapy with αPD-L1 in AMM by single cell RNA sequencing.
Bone marrow was collected from AMM patient before and after 2 cycles (6weeks) of therapy with atezolizumab. CD138 negative bone marrow mononuclear cells obtained pre therapy and 6 weeks post therapy were characterized using scRNA-Seq. A. t-SNE plot with 9 distinct populations determined by unsupervised clustering. Figure also shows distribution of the immune cells from pre therapy bone marrow (Pre) and post therapy bone marrow (Post). B. Percent of immune cells from pre therapy (Pre) and post atezolizumab therapy (Post) within the clusters shown in Figure 3E.

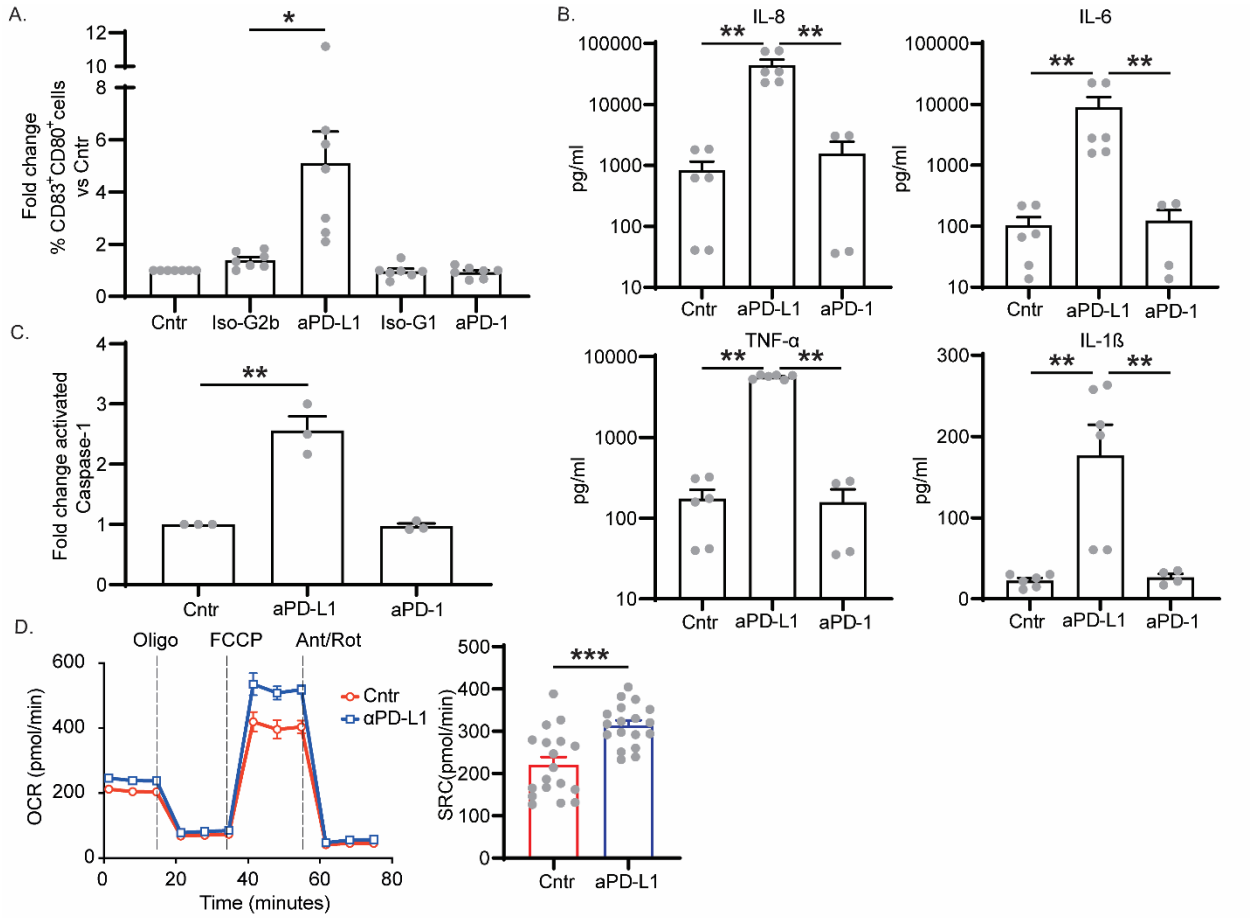

Figure 8: PD-L1 blockade leads to functional changes in dendritic cells.
Immature Mo-DCs were either left untreated (control, Cntr) or treated with either anti-PD-L1 antibody (200µg/ml), anti-PD-1 antibody (200µg/ml) or their respective isotype control antibodies (Ig-G2b and Ig-G1) at 200µg/ml. Culture supernatants were analyzed for changes in cytokines using Luminex assay. Representative data from 7 healthy donors (HDs). A. DC maturation following treatment with either anti-PD-L1, anti-PD-1 or isotype control. Figure shows fold change in CD83 and CD80 double positive DCs compared to untreated cells. B. Changes in secreted IL-8, IL-6, TNF-α and IL-1ß following treatment with anti-PD-L1 or anti-PD-1. C. Treatment with anti-PD-L1 leads to early activation of Caspase-1. Fold change of activated Caspase-1 in immature Mo-DCs following treatment with anti-PD-L1 or anti-PD-1 for 4 hours. Figure shows fold change compared to untreated cells (Cntr). D. Changes in respiratory capacity of DCs following treatment with anti-PD-L1. Immature Mo-DCs (n=3 HDs) were either left untreated (control; Cntr) or were treated with anti-PD-L1 (200µg/ml for 3 hrs) and their spare respiratory capacity was analyzed using Seahorse XFe96 analyzer. Basal, coupled, maximal and spare respiratory capacity was analyzed. Line graph shows data from a representative patient. Bar graph on the right shows data from all 3 different donors (mean+/-SEM). (*p<0.05, **p<0.01, ***p<0.001; A,C,D=Mann-Whitney U test, B=Kruskall Wallis test).

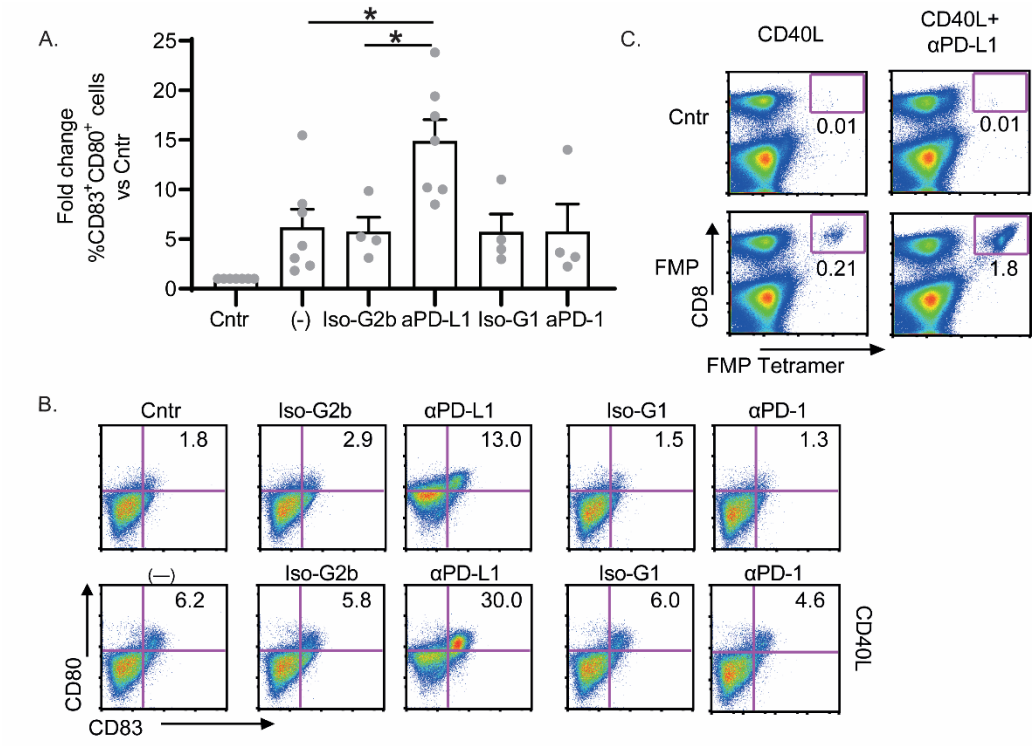

Figure 9: PD-L1 blockade synergizes with CD40L to improve antigen specific T cell expansion. Immature Mo-DCs were either left untreated (control, Cntr) or treated with either anti-PD-L1 antibody (200µg/ml), anti-PD-1 antibody (200µg/ml) or their respective isotype control antibodies (Ig-G2b and Ig-G1) at 200µg/ml or CD40L (250ng/ml). Culture supernatants were analyzed for changes in cytokines using Luminex assay. Representative data from 7 healthy donors (HDs). A. Anti-PD-L1 treatment synergizes with CD40L to improve DC maturation. Figure shows fold change in DC maturation (assessed by increase in CD83 and CD80 double positive cells) compared to control cells. B. Representative data from one donor showing increased DC maturation with concurrent treatment with CD40L and PD-L1. C. Immature Mo-DCs (HLAA2.1+) were stimulated with CD40L alone or CD40L + anti-PD-L1 antibody. After overnight culture, DCs were loaded with HLAA2.1 specific influenza matrix peptide (FMP) at 0.1µg/ml and used to stimulate autologous T cells. After 10-12 days of DC:T cell co-culture, expansion of influenza specific T cells was analyzed using FMP specific tetramer. (*p<0.05, Kruskal Wallis test)